



Effect of radiation on laminar natural convection of nanofluid in a vertical channel with single- and two-phase approaches

Amir Mostafazadeh¹ · Davood Toghraie¹ · Ramin Mashayekhi² · Omid Ali Akbari²

Received: 17 February 2019 / Accepted: 3 April 2019 / Published online: 24 April 2019
© Akadémiai Kiadó, Budapest, Hungary 2019

Abstract

In the present study, heat transfer and laminar flow of a nanofluid in a vertical channel by considering the effect of radiation with single- and two-phase approaches with prescribed surface temperature conditions and prescribed surface heat flux conditions were simulated. The main goal of this study is to investigate the effect of variations of Grashof number (Gr), radiation parameter (Nr) and volume fraction of nanoparticles (ϕ) on flow and heat transfer characteristics. For this goal, flow with $Gr = 5, 10, 15$ and 20 , volume fractions of $0, 0.1$ and 0.2 and radiation parameters of $Nr = 0, 0.5$ and 1 were simulated. The results show that by increasing Grashof number in both cases of constant heat flux and temperature, nanofluid velocity increases and in both cases of constant temperature and heat flux by increasing volume fraction, the velocity and temperature of the nanofluid drops. The presence of moving wall (plate boundary condition) induces secondary flows in the flow field, and the flow movement in the channel will experience drift because of temperature variations and buoyancy forces due to inducement of secondary forces and the effect of penetration of moving plate velocity into the fluid close by it which will affect the entire fluid flow field in the end. For fixed plate case, the velocity of nanofluid at the walls is zero because of fixed position of the plate and presence of no-slip boundary condition on the solid walls. By increasing the applied temperature, the value of kinetic and internal energy of the velocity field rises which results in higher density gradients and higher buoyancy forces. For both constant heat flux and temperature, increasing solid nanoparticles volume fraction results in lowering of the velocity contour elevations. The quantitative level of axial velocity curves for constant heat flux condition compared with constant temperature case for $Gr = 5$ and $Nr = 0.5$ is about 2–3 times less. For constant temperature boundary condition, for $Gr = 5$ and $Nr = 0.5$ and volume fraction of 0.1% , the maximum velocity happens at regions 30–50% of channel height from the bottom.

Keywords Heat transfer · Nanofluid · Radiation · Two phases · Single phase

Introduction

Convective heat transfer in vertical channels is important to improve cooling systems, exchangers, energy geo-structures, solar cells, nuclear reactors and many more fields. Based on the trends in micro and nano areas, creation of smaller devices has become possible. One of the proper

methods for cooling these devices is using nanofluid as a coolant material. Based on this approach, studying heat transfer and flow of nanofluid in different geometries has been carried out by many scientists in the past decades. Das et al. [1] studied transient natural convection inside a vertical channel filled with nanofluid by considering thermal radiation. The governing fluid equation was studied by using exact solution method for the determination of velocity and temperature of the nanofluid for prescribed surface temperature (PST) and prescribed surface heat flux (PHF) cases. The result showed that fluid velocity is higher in PST case compared with PHF case. Pantokratoras [2] studied natural convection along a vertical isothermal plate by considering linear and nonlinear Rosseland thermal radiation. He showed that the temperature profile follows a

✉ Davood Toghraie
Toghraee@iaukhsh.ac.ir

¹ Department of Mechanical Engineering, Khomeinishahr Branch, Islamic Azad University, Khomeinishahr 84175-119, Iran

² Young Researchers and Elite Club, Khomeinishahr Branch, Islamic Azad University, Khomeinishahr, Iran

special S-shaped pattern. Also, by increasing shear stress at the wall, heat transfer of the wall decreases. Hossain and Tashakor [3] investigated the effect of mixed convection along a plate with uniform surface temperature. In their numerical work, the equations were discretized with a finite difference method. They showed that in all cases the shear stress and local heat transfer can increase by increasing radiation constant and increases by increasing heat transfer Prandtl number and shear stress it decreases. Das et al. [4] considered the effect of radiation on transient cavity flow between two parallel vertical plates. They reached the conclusion that velocity and temperature of the fluid decrease by increasing Prandtl number. Also by increasing Grashof number, the velocity rises. Das et al. [5] simulated convective boundary condition for nanofluid flow. They studied heat and mass transfer of an incompressible and electrical conductor nanofluid flowing on a warmed plate with convective boundary condition. They reached the conclusion that increasing surface convection, heat radiation and Brownian motion parameters leads to increased thickness of the boundary layer. Dogonchi and Ganj [6] considered MHD buoyancy flow and heat transfer on a spread plate in the presence of thermal radiation by considering Brownian motion. Their results showed that distribution of fluid velocity and temperature decreases by increasing radiation parameter. Rashidi et al. [7] considered transient heat transfer of nanofluid over a stretching sheet in the presence of magnetic field and heat radiation and studied the effects of buoyancy. The results for water–CuO nanofluid showed that increasing buoyancy force results in increased velocity and reduced temperature and by increasing volume fraction the fluid velocity decreases. Pantokratoras and Fang [8] investigated the effect of thermal radiation on laminar flow along a moving plate. In this present study, the temperature difference between the sheet and flow was considered to be negligible and the Rosseland thermal radiation was used for analysis and mathematical solution of radiation equations. They reached the conclusion that Rosseland approximation is correct for small temperature difference between fluid and sheet. Prandtl number and radiation number both have a similar effect on temperature profile. When the Prandtl number is increased the temperature profile becomes linear and changes from S shape to normal shape. Garoosi et al. [9] studied mixed convection heat transfer in a square cavity with a two-phase mixture method. Their results showed that for small Richardson numbers, the effect of increasing heating and cooling number will result in increased heat transfer rate. Also by decreasing nanoparticle thickness, the natural heat transfer rate increases. Akbarinia and Behzadmehr [10] considered laminar mixed convection in a horizontal curved tube containing water aluminum nanofluid with the two-phase mixture method and they

reached the conclusion that for a given Reynolds number, buoyancy force has a negative effect on the Nusselt number whereas the concentration of nanoparticles has a positive effect on increasing heat transfer and also has a reducing effect on surface friction. Mirmasoumi and Behzadmehr [11] performed a numerical simulation of laminar mixed convection of nanofluid in a horizontal tube with the two-phase mixture method. They reached the conclusion that the nanofluid concentration in the fully developed region does not have an effect on hydrodynamic parameters but has a strong influence on thermal properties. Also above the tube and close to the wall, the nanofluid concentration was higher. Shariat et al. [12] performed simulation of natural and forced convection in an elliptic duct via the two-phase mixture method and realized that in the fully developed region the buoyancy force and particle momentum do not have a high effect on velocity profile. Also by decreasing nanoparticles size and increasing Richardson number, the secondary flows are reinforced and they increase. Oztop et al. [13] used the heat line analysis method for heat transfer in a square inclined enclosure with non-uniform heating for copper nanofluid with water as base fluid. The equations were solved with the finite element method. The results showed that the heat transfer rate of the cavity rises by increasing nanoparticles and this increase will be higher for cavities with lower Rayleigh number. Xu et al. [14] considered fully developed laminar flow between two straight vertical plates filled with a nanofluid. It was determined that heat transfer properties can become significantly higher by using nanofluid. Ahmed et al. [15] considered mixed convection due to two discrete heat sources in a cell with two adjacent moving walls filled with nanofluid. In this experiment, the copper, silver oxide and thallium oxide nanoparticles were used. They studied the effect of different parameters such as Richardson number, fluid type and position of heater and concluded that Nusselt number decreases along the position of heat source and increases by increasing volume fraction of particles. Joshaghani et al. [16, 17] studied the effect of heat transfer in the ground as a result of ground heat exchangers and energy geo-structures. In other studies, they studied the flow and heat transfer in microchannels [18, 19].

In recent years, extensive studies have been carried out on heat transfer. Most of these studies are in nanofluidic [20–27], two-phase flow treatment using different methodologies such as SPH [28, 29] and LBM [30, 31]. Many studies have also examined the heat transfer in various geometries [32, 33]. In this study, the laminar nanofluid flow in a vertical channel was considerably including radiation. Contrary to the majority of previous studies which used exact solution, here the numerical solution and Rosseland method were used to investigate the

effect of radiation on the nanofluid. Also, along with single-phase approach the two-phase mixture method was also used to investigate flow and heat transfer characteristics of nanofluid in constant temperature and constant heat flux boundary conditions. Also, fixed and moving walls were used.

Geometry of the problem

In this study, a numerical investigation of effect of heat radiation on natural and steady convection of nanofluid in a vertical channel was done with two-phase mixture and single-phase methods. Figure 1 shows the problem geometry. Two parallel plates with fixed distance along the x -axis are used and the channel entrance is situated along y -axis. The channel is vertical and the variations are studied along the width of the channel. At first, fluid and wall are of the same temperature equal to T_h which is constant. At time $t > 0$, the plate $y = 0$ moves with velocity λu_0 ($\lambda = 0$ for stationary case and $\lambda = 1$ for moving case) and the plate temperature falls or rises so that it reaches temperature T_0 in PST case. In PHF case, the rate of transferred heat to plate $y = 0$ is constant. The fluid motion is solely influenced by motion of $y = 0$ plate and buoyancy force. The fluid momentum is linearly proportional with buoyancy force. The nanofluid in this study is water and copper nanoparticles, and the numerical simulation of this study was done with finite volume method [34–45]. It should be stated that heat transfer due is because of radiation and natural convection. The important parameters for numerical solution are Grashof number Gr of 5, 10, 15 and 20, radiation parameter Nr of 0, 0.5 and 1, volume fraction ϕ of 0, 0.1 and 0.2% and Prandtl number of $Pr = 0.2$ in the room temperature, and the flow is modeled in laminar regime.

For analyzing the nanofluids in a single-phase approach, the behavior of solid particles in the liquid is taken to be the same as the primary phase (liquid). Under this

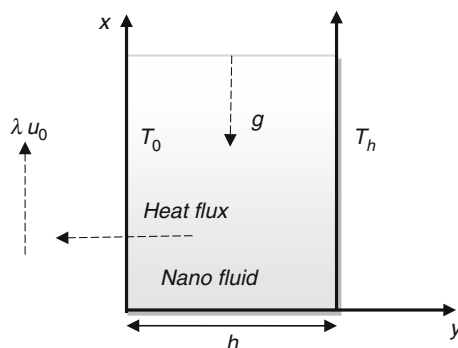


Fig. 1 Schematic of the considered problem

assumption, there is no deviation in the motion between solid phase (particles) and liquid and to a large extent the nanofluid is modeled as a regular fluid. The justification for this is the very small size of nanoparticles and their continuous motion along with the fluid. Also the results of this study also apply to the two-phase mixture method. This numerical study is done by considering Newtonian fluid in both cases in steady state.

Governing equations

Fundamental equations for a single-phase case

For incompressible fluid with assumption of uniform dispersion of particles in the fluid and assumption of Newtonian behavior of the nanofluid and using the Boussinesq approximation, the fundamental equations of continuity, momentum and energy become [46]:

Continuity:

$$\nabla \cdot \vec{V} = 0 \quad (1)$$

Momentum:

$$\rho_{nf} \frac{D\vec{V}}{Dt} = -\nabla P + \mu_{nf} \nabla^2 \vec{V} + \vec{F} \quad (2)$$

In the above equation, \vec{F} is the vector of body force.

Energy:

$$(\rho C_p)_{nf} \frac{DT}{Dt} = k_{nf} \nabla^2 T + \mu_{nf} \phi - \nabla q_r \quad (3)$$

In the above equation, q_r refers to heat radiation flux. This radiation heat flux vector in a gray model can be approximated with the following equation,

$$q_r = -\Gamma \nabla G \quad (4)$$

And the coefficient Γ can be obtained from,

$$\Gamma = \frac{1}{\alpha(3 + \sigma_s) - (C\sigma_s)} \quad (5)$$

where σ_s is dispersion coefficient and C is the coefficient of linear anisotropic phase function. In Eq. (4), G is implicit radiation. Implicit radiation is calculated from the following relationship:

$$G = 4\sigma n^2 T^4 \quad (6)$$

In Eq. (6), σ is Stefan Boltzmann constant equal to $(5.67 \times 10^{-8} \frac{W}{m^2 K^4})$ and n is refractive index. Based on the value of G in a thick medium, the radiation flux emitted can be calculated from,

$$q_r = -16\sigma \Gamma T^3 \nabla T \quad (7)$$

Since this radiation heat flux has the same form as the Fourier conduction law, we can write:

$$q = q_c + q_r = -(k + k_r) \nabla T \quad (8)$$

where k is the thermal conductivity and k_r is radiation conduction factor. Based on Eq. (8), we have,

$$k_r = 16\sigma \Gamma T^2 \quad (9)$$

Governing equations for the two-phase mixture method

This model is used for two or several fluid or particle phases. Therefore, its application is suitable for nanofluid. The mixture model uses a combined momentum equation so that the average properties of the different phases are considered in the equation. In the following, the governing equations for the two-phase method are presented. The explanations for Navier–Stokes equations are different in the two-phase case and given by the following [47, 48],

Continuity:

$$\nabla \cdot \vec{V}_m = 0 \quad (10)$$

Momentum:

$$\begin{aligned} \nabla_{\rho m} \cdot \vec{V}_m \vec{V}_m = \nabla \cdot \mu_m \nabla \vec{V}_m + \nabla \cdot \left[\sum_{k=1}^n \phi_k \rho_k \vec{V}_{dr,k} \right] \\ + (\rho\beta)_m (T - T_h) g \end{aligned} \quad (11)$$

Energy:

$$\nabla \cdot \left[\sum_{k=1}^n (\rho_k c_{pk}) \phi_k \vec{V}_k T \right] = \nabla \cdot k_m \nabla T - \nabla \cdot q_r \quad (12)$$

In Eqs. (13)–(17), subscript k represents summation index, dr represents drift, p represents solid particles, f represents fluid and m represents nanofluid mixture. In the preceding equations, different velocities were defined, and Eqs. (26) to (30) describe the method of calculating them [49]:

Average mass velocity [50, 51]

$$\vec{V}_m = \frac{\sum_{k=1}^n \phi_k \rho_k \vec{V}_k}{\rho_m} \quad (13)$$

Drift velocity for the second phase,

$$\vec{V}_{dr,k} = \vec{V}_k - \vec{V}_m \quad (14)$$

Relative velocity of the two phases:

$$\vec{V}_{pf} = \vec{V}_p - \vec{V}_f \quad (15)$$

Drift velocity proportional with relative velocity:

$$\vec{V}_{dr,p} = \vec{V}_{pf} - \sum_{k=1}^n \frac{\phi_k \rho_k}{\rho_m} \vec{V}_{fk} \quad (16)$$

Relative velocity v_{pf} can be obtained from the following equations using the definition of drag function:

$$\begin{aligned} \vec{V}_{pf} = \frac{\rho_p d_p^2 (\rho_p - \rho_m)}{18 \mu_f f_{drag} \rho_p} (g - (\vec{V}_m \cdot \nabla) \vec{V}_m) \\ f_{drag} = \begin{cases} 1 + 0.15 Re_p^{0.687} & (Re_p \leq 1000) \\ 0.0183 Re_p & (Re_p > 1000) \end{cases} \end{aligned} \quad (17)$$

All of the expressed equations in the preceding two sections require thermophysical properties of water and copper particle which are briefly given in Table 1.

Properties of nanofluid for single-phase case

Dynamic viscosity of the nanofluid [52]:

$$\mu_{nf} = \frac{\mu_f}{(1 - \phi)^{2.5}} \quad (18)$$

Nanofluid density [53–57]:

$$\rho_{nf} = (1 - \phi) + \phi \rho_s \quad (19)$$

Specific heat capacity of the nanofluid [58–60]:

$$(\rho c_p) = (1 - \phi)(\rho c_p)_f + \phi(\rho c_p)_s \quad (20)$$

Thermal expansion coefficient for the nanofluid:

$$(\rho\beta)_{nf} = (1 - \phi)(\rho\beta)_f + \phi(\rho\beta)_s \quad (21)$$

Thermal conductivity of the nanofluid [61]:

$$k_{nf} = \frac{[k_s + 2k_f - 2(k_f - k_s)]}{[k_s + 2k_f + \phi(k_f - k_s)]} \quad (22)$$

Table 1 Thermophysical properties of water–copper [49]

Thermophysical properties	Water	Copper
Density $\rho/\text{kg m}^{-3}$	997.1	8993
Dynamic viscosity $\mu/\text{Pa s}$	909.4e–6	–
Kinematic viscosity $\nu/\text{m}^2 \text{s}^{-1}$	0.912e–6	–
Specific heat $C_p/\text{J kg}^{-1} \text{K}^{-1}$	4179	385
Thermal conductivity $k/\text{W mK}^{-1}$	0.613	401
Thermal expansion coefficient β/K^{-1}	210e–6	16.7e–6
Molecular weight/ g mol^{-1}	18.5152	79.54

In these equations, the subscript *s* refers to particle properties (copper), *f* refers to base fluid (water) and *nf* refers to nanofluid.

Nanofluid properties in the two-phase approach

The thermophysical properties of the nanofluid are different in the two-phase approach, and they are calculated via the following relationships [62]:

Heat capacity:

$$(\rho c_p)_m = (1 - \phi_p)(\rho c_p)_f + \phi_p(\rho c_p)_p \tag{23}$$

Density:

$$\rho_m = (1 - \phi_p) + \phi_p \rho_p \tag{24}$$

Thermal expansion coefficient:

$$(\rho\beta)_m = (1 - \phi_p)(\rho\beta)_f + \phi_p(\rho\beta)_p \tag{25}$$

where *p* represents solid particles, *f* represents fluid and *m* represents nanofluid mixture. The dimensionless equations for temperature–position–velocity are as follows [1]:

Dimensionless (transverse) position:

$$\eta = \frac{y}{h} \tag{26}$$

Dimensionless velocity:

$$u_1 = \frac{u}{u_0} \tag{27}$$

Dimensionless temperature for PST case:

$$\theta = \frac{T - T_h}{T_0 - T_h} \tag{28}$$

Dimensionless temperature for PHF case:

$$\theta = \frac{k_f(T - T_h)}{q_w h} \tag{29}$$

where q_w refers to heat flux of the wall. Grashof number for PST case is defined as,

$$Gr = \frac{g\beta_{nf}(T - T_h)h^2}{u_0\nu_f} \tag{30}$$

And for PHF case:

$$Gr = \frac{g\beta_{nf}q_w h^3}{u_0 k_{nf} \nu_f} \tag{31}$$

The radiation number *Nr* which shows the radiation capacity divided by surface convection capacity [1]:

$$Nr = \frac{16\sigma T_\infty^3}{3k_{nf}k^*} \tag{32}$$

In this equation, σ is the Boltzmann constant, k_{nf} is thermal conductivity and k^* is Rosseland absorption coefficient.

Method of numerical solution

Boundary conditions

The solution is done for two cases of fixed wall and wall moving with constant velocity of u_0 . At the start of the solution, the two walls are situated at $y = 0$ and $y = h$ and the flow between them is in thermal equilibrium with temperature T_h . After starting the solution in the PST case, the temperature of the lower wall reaches T_0 and in the PHF case it reaches the constant heat flux q_w . The boundary conditions are given in Eqs. (33)–(35),

$$u = 0, \quad T = T_h, \quad 0 < y < h \tag{33}$$

$$u = \lambda u_0, \quad T = T_0(\text{PST}), \quad k_{nf} \frac{\partial T}{\partial y} = -q_w, \quad y = 0(\text{PHF}) \tag{34}$$

$$u = 0, \quad T = T_h, \quad y = h \tag{35}$$

The boundary conditions in this study are shown for the 2D and 3D cases in Fig. 2.

Method of solving equations

For solving the equation, the solver based on pressure is used and the problem is solved for a steady-state case by considering heat radiation and application of two-phase mixture and single-phase methods. These simulations were done with the finite volume method and in 3D coordinates. For solving the numerical domain, the SIMPLEC algorithm [63–68] was used for velocity–pressure coupling. In this method, the equations of the velocity and pressure are modified to establish the mass conservation principle and to obtain the pressure field. Also, in the current investigation, PRESTO method was utilized for intuiting the pressure. This method is used for highly rotational flows, the

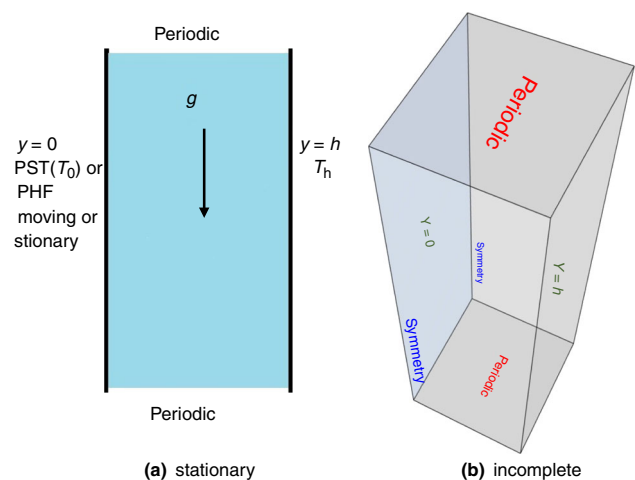


Fig. 2 Model and boundary conditions for 2D and 3D cases

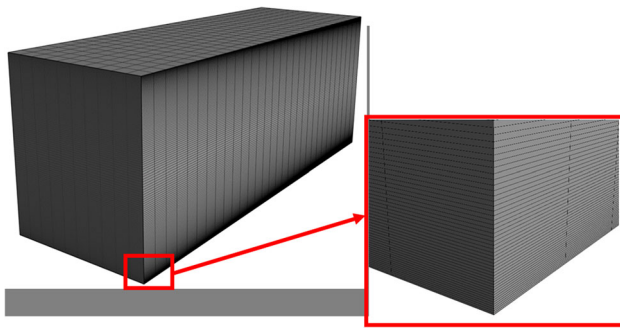


Fig. 3 Demonstration of computational mesh

Table 2 Effect of number of network elements on average velocity

Number of elements	Average velocity/(m/s)	Deviation/%
6000	4.2e-5	11.3
15,000	3.28e-5	9.76
30,000	3.46e-5	4.76
45,000	3.5e-5	2.02
60,000	3.45e-5	0.883

flows with very intense pressure gradients or in much curved domains. Also, the second-order upwind approach was used for solving the equations. The convergence criterion is when the residual curve reaches accuracy of 10^{-9} and in all analyses and convergences for velocity and average temperature in the solution space the solving accuracy is 10^{-9} .

Figure 3 shows the mesh used in this problem. Based on the boundary conditions of the problem, in order to better evaluate flow parameters close to the two walls $\eta = h$ and $\eta = 0$ the density of mesh close to walls was higher and for reaching this goal an organized uniform mesh was used for making geometric cells.

The effect of number of grid points on velocity was checked so that it is independent with respect to the base mesh and all analysis was considered for volume fraction of 0.1 for the average velocity in the stationary plate case. The acceptable error is below 1% and used as a benchmark for verifying the solution and using 60,000 elements satisfies this criterion. Table 2 shows the effect of number of grid points on average velocity. It is seen that from 60,000 the criterion for error below 1% holds and for more elements the results stay the same; therefore, 60,000 elements is the condition for independence of results from the mesh.

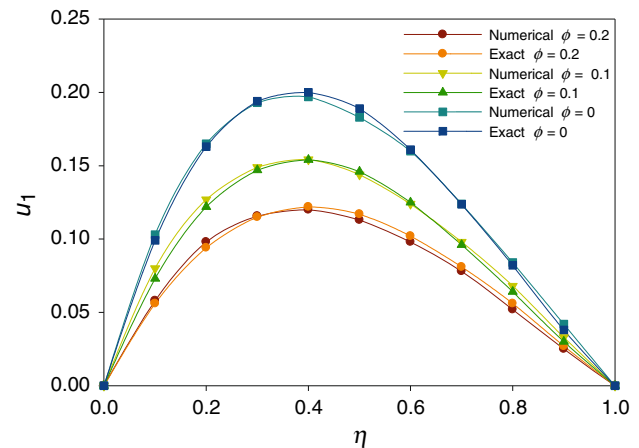


Fig. 4 Comparison of two-phase numerical solution for the case of fixed wall and temperature for $Gr = 5$ and $Nr = 0.5$ and volume fractions of 0, 0.1 and 0.2% with the exact solution of Ref. [1]

Validation

Figure 4 shows the comparison of dimensionless velocity across the width for the results of numerical and exact solutions from Ref. [1] for case of fixed wall and constant temperature and $Gr = 5$ and $Nr = 0.5$ for different volume fractions. For the exact solution, the problem was considered to be transient and single phase. The value of error among the curves was less than 5% which is acceptable.

Results and discussion

Effect of volume fraction on velocity

Figure 5 shows the results of solving the numerical field for the single-phase and two-phase cases for the nanofluid flow in the channel with both PST and PHF boundary conditions. This investigation is done for $Gr = 5$ and $Nr = 0.5$. For base fluid and different volume fractions of 0, 0.1 and 0.2 solid nanoparticles, the variations in axial velocity field in a constant section were considered. The goal was to follow the effect of changing solid nanoparticles volume fraction and type of heat boundary condition on axial velocity field of the fluid. As it can be seen, the velocity of the nanofluid is zero at solid walls because the plate is stationary and no-slip boundary condition exists.

Based on the behavior of curves in Fig. 5, increasing solid nanoparticles volume fraction results in reduced elevation of velocity curves. The reason for this behavior is increased volume fraction of solid nanoparticles in the base fluid which results in a higher viscous force and density for the coolant fluid and reduces buoyancy force. This behavior is shown in curves of Fig. 5 for both single- and two-phase simulations. Based on velocity curves, the

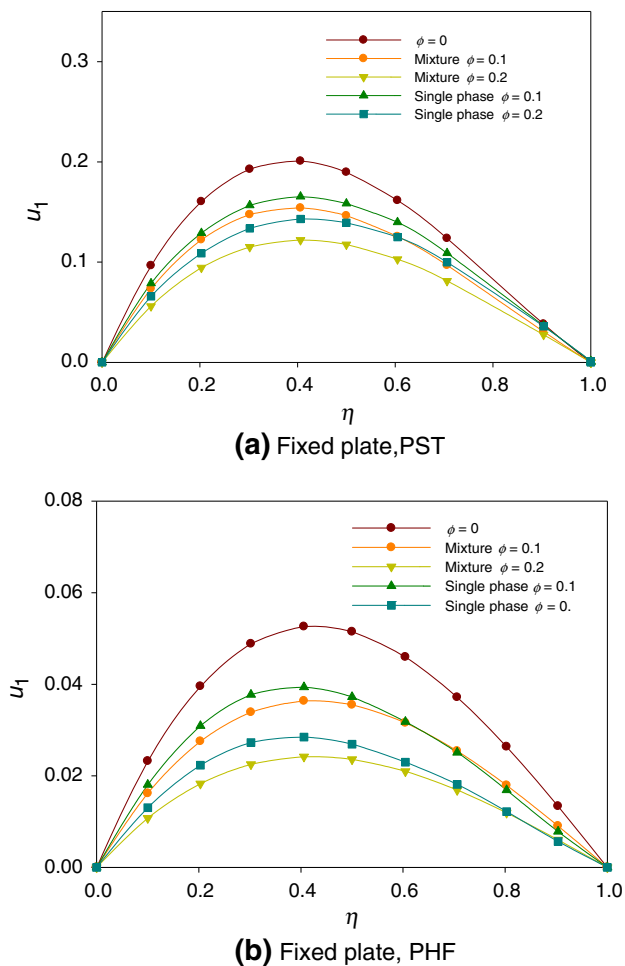


Fig. 5 Variations of dimensionless velocity across the channel width for **a** fixed plate and constant temperature condition and **b** constant heat flux for $Gr = 5$, $Nr = 0.5$ and different volume fractions

changes in velocity values based on the selected model are identical for PST boundary condition for zero volume fraction of nanoparticles but for the constant flux boundary condition this is not true. Also the quantitative levels of axial velocity curves for constant flux case are about 2–3 times lower than constant temperature case. This is because in the same Grashof number, the constant temperature boundary condition applies more heat to the flow field compared with constant flux case so that by increasing the prescribed temperature to the fluid the value of internal and kinematic energy of the velocity field rises and results in stronger gradients and increases buoyancy force. The calculation of the change in value of velocity in the channel center ($\eta = 0.5$) for single- and two-phase cases is given in Table 3. The value of this difference for PST case for volume fraction of 0.2% solid nanoparticles is about 18.8% and for 0.1% volume fraction it is about 8.2%. This behavior for PHF case is 12.5% for volume fraction of 0.2% solid nanoparticles and 5% for 0.1 volume fraction.

In general, for both cases of constant flux and temperature the determination of flow field behavior results in higher value in the single-phase method.

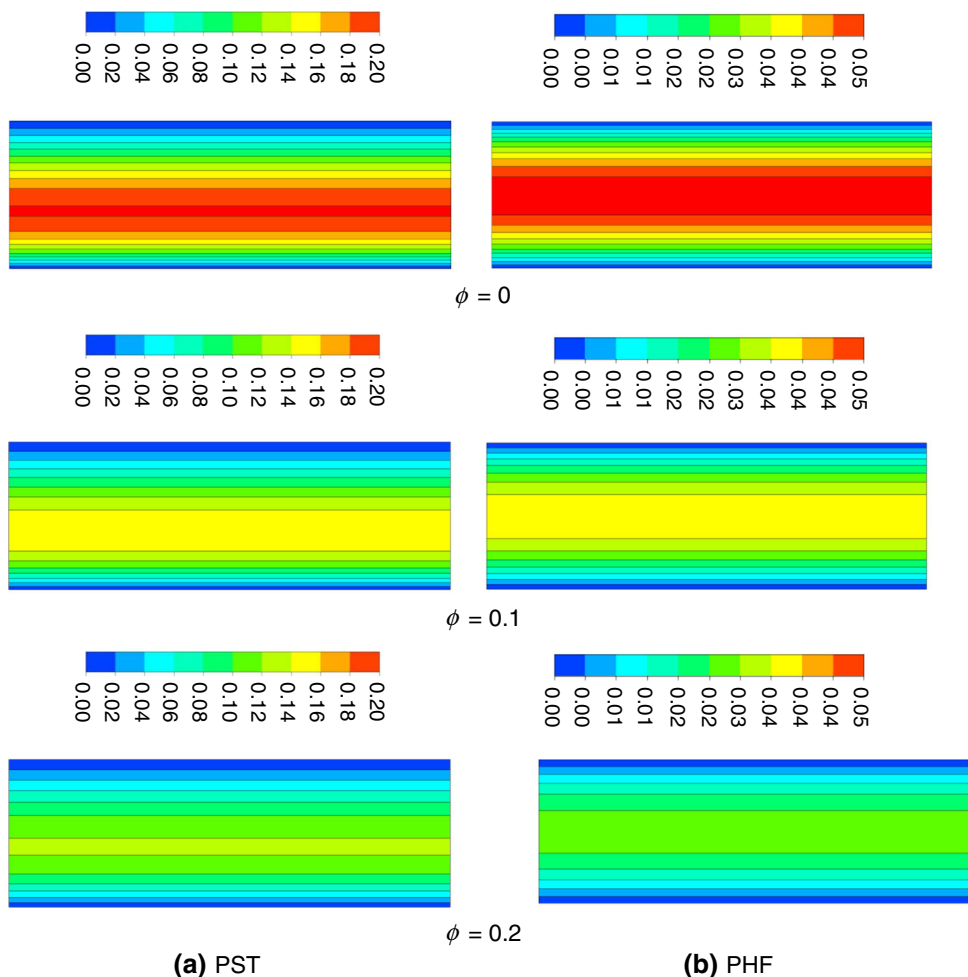
In Fig. 6, the velocity contours for simulation of velocity field for the two-phase method and constant temperature and heat flux boundary conditions for volume fractions of 0, 0.1 and 0.2% for $Gr = 5$ and $Nr = 0.5$ are shown separately. It is observed that for the base fluid, the highest value of velocity occurs in the hydrodynamic flow field. The reason is that the viscous force between fluid layers of base fluid is smaller. Also, in the fluid with higher volume fraction the viscous force is the highest and the lowest velocities are obvious. Based on velocity contours for constant temperature BC due to temperature difference between the lower and upper plate of the channel, the axial velocity distribution is asymmetrical and the maximum temperature is toward the wall with the higher heat so that for all three contours in Fig. 6 the maximum velocity in the constant temperature case happens at 30–50% of the channel height but for constant heat flux case the velocity field is nearly symmetrical.

In Fig. 7, the dimensionless velocity curves are drawn for PST (prescribed temperature) and prescribed heat flux (PHF) boundary conditions when the lower plate is moving. The results are displayed for $Gr = 5$, $Nr = 0.5$ and volume fractions of 0, 0.1 and 0.2 along channel width. This diagram shows the effect of changes in solid nanoparticles volume fraction on dimensionless axial velocity and the effect of movement of the lower plate on the flow field. Similar to the velocity curves for fixed plate boundary condition, by increasing solid nanoparticles volume fraction, because of increased viscous force the axial force is reduced. But for the hot moving plate with both boundary conditions, the variations in axial velocity have a smaller sensitivity to the modeling type (single-phase or two-phase). This, however, shows a great distinction for fixed plate in the previous curves. The axial velocity curves are affected by the thermal boundary condition, and the curves are specially changed in regions closed to the moving sheet. In addition to the hot sheet movement, imposing constant temperature also results in higher velocity and deeper penetration of hot plate movement into the neighboring fluid and in these regions the stability of plate motion or dimensionless velocity equal to 1 ($u_1 = 1$) covers about 10% of regions in proximity to the moving plate based on Fig. 7a. The dimensionless axial velocity curves with the constant heat flux boundary condition according to Fig. 7b result in a more uniform velocity profile for all volume fractions and smaller distinction between single- and two-phase methods so that by increasing solid nanoparticles volume fraction the behavior of dimensionless axial velocity tends to a linear shape.

Table 3 Comparison of the results of dimensionless velocity values for single- and two-phase models for fixed plate, constant heat flux and temperature for section of $\eta = 0.5$ for $Gr = 05$, $Nr = 0.5$ and volume fractions of 0.1 and 0.2%

Boundary condition	Deviation/%	Mixture	Single phase	Volume fraction
PST	8.2	0.158	0.146	0.1
	18.8	0.117	0.139	0.2
PHF	5	0.0361	0.384	0.1
	12.5	0.0240	0.0277	0.2

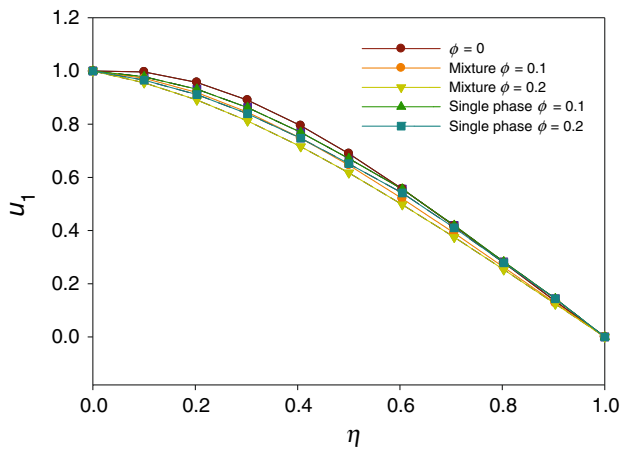
Fig. 6 Dimensionless velocity contour for **a** fixed plate and constant temperature and **b** stationary plate and fixed thermal flux for section $\eta = 0$ for $Gr = 5$ and $Nr = 0.5$ and different volume fractions



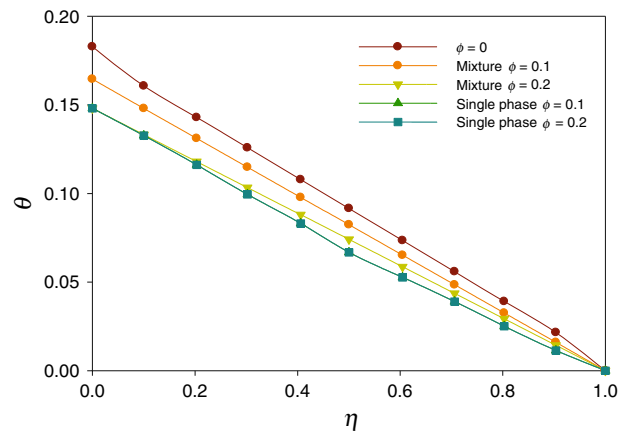
In Table 4, the values of axial velocity for channel centerline ($\eta = 0.5$) for both single- and two-phase conditions for $Gr = 5$, $Nr = 0.5$ and PST (constant temperature) and PHF (constant flux) boundary conditions are compared. Based on the considered values in Table 4, there is a clear difference between axial velocity curves and this parameter shows a distinctive behavior for each volume fraction for the constant temperature boundary condition; however, the distinction is rather limited for the constant heat flux BC case.

Effect of changing volume fraction on temperature

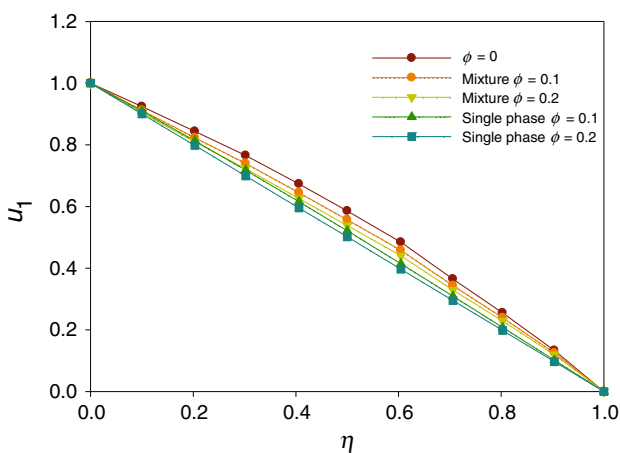
In Fig. 8, the dimensionless temperature field across channel field for $Gr = 5$ and $Nr = 0.5$ for single- and two-phase models for volume fractions of 0, 0.1 and 0.2% solid nanoparticles for constant temperature and heat flux boundary conditions are shown. Figure 8 shows that adding solid nanoparticles volume fraction in the cross section for constant heat flux case (in fixed and moving plate case) has an inverse effect on changes on dimensionless temperature



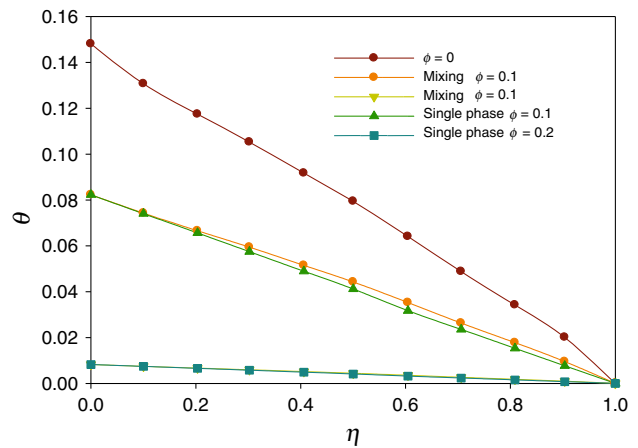
(a) Moving plate, PST boundary conditions



(a) Fixed plate, PHF boundary conditions



(b) Moving plate, PHF boundary conditions



(b) Moving plate, PHF boundary conditions

Fig. 7 Variations of dimensionless velocity across channel width for conditions of **a** moving plate and constant temperature and **b** moving plate and constant heat flux for $Nr = 0.5$, $Gr = 5$ and different volume fractions

Fig. 8 Variations in dimensionless temperature in the channel width for condition of **a** fixed plate and constant heat flux and **b** moving plate and constant heat flux for $Gr = 5$ and $Nr = 0.5$ and different volume fractions

so that by adding volume fraction, a reduction in temperature field and an increase in channel cooling are observed. This is in accordance with physical behavior of the nanoparticles, and as a result, it is an optimum property which can be applied in industrial cooling because nanoparticles increase heat absorption and because of better heat conduction coefficient transmits heat faster than

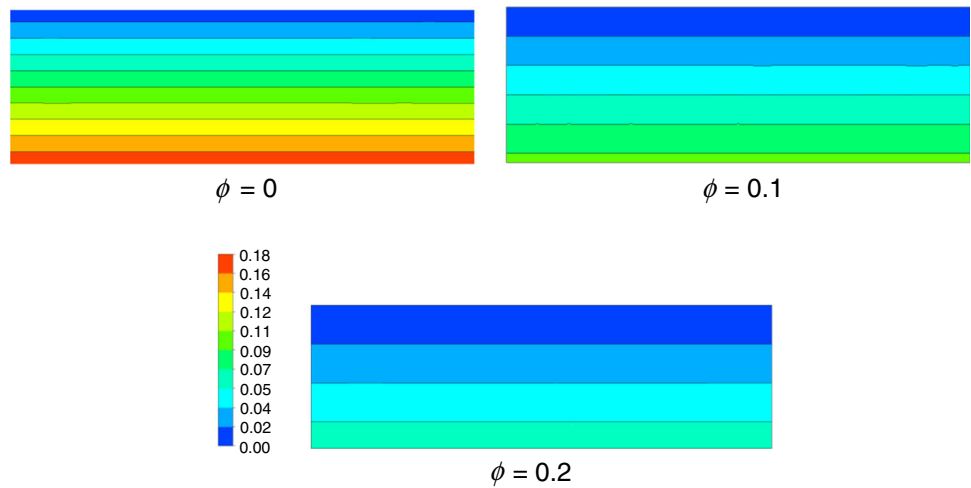
substrate fluid and therefore reduces fluid temperature and the temperature distribution becomes more uniform upon adding solid nanoparticles with higher volume fraction.

The dimensionless temperature contours for the two-phase case for moving plate and constant heat flux case are shown in Fig. 9 which shows temperature distribution in the channel for different volume fractions. In these

Table 4 Comparison of dimensionless velocity results for single-phase and two-phase models for conditions of moving plate, constant heat flux and temperature at section $\eta = 0.5$ for Grashof number $Gr = 5$ and radiation number $Nr = 0.5$ and different volume fractions of 0.1 and 0.2%

Boundary condition	Deviation/%	Mixture	Single phase	Volume fraction
PST	4.6	0.64	0.57	0.1
	6.5	0.61	0.65	0.2
PHF	6.9	0.5212	0.5563	0.1
	6	0.5014	0.5386	0.2

Fig. 9 Temperature distribution in the channel for different volume fractions and $Gr = 5$, $Nr = 0.5$ and $\eta = 0$



contours, the most uniform temperature distribution happens for the highest solid nanoparticles volume fraction and formation of hot zones is observed in the base fluid.

Figure 10 shows dimensionless temperature profile for fixed and moving plates for PST boundary condition. This analysis is shown for $Gr = 5$, $Nr = 0.5$ and different solid nanoparticles volume fractions. This curve is observed to be pseudo-linear, and most data in single- and two-phase cases for moving wall coincide with each other and along the channel width, by moving away from the hot wall the temperature drops. This means that the temperature field in the introduced conditions is almost independent of the dynamic plate BC and solid nanoparticles volume fraction.

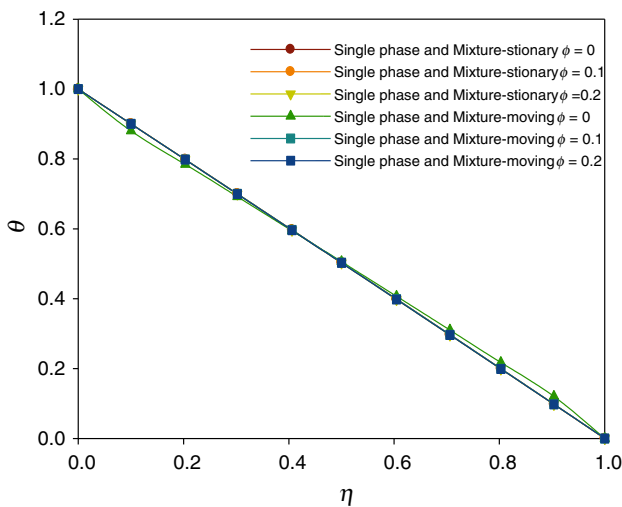
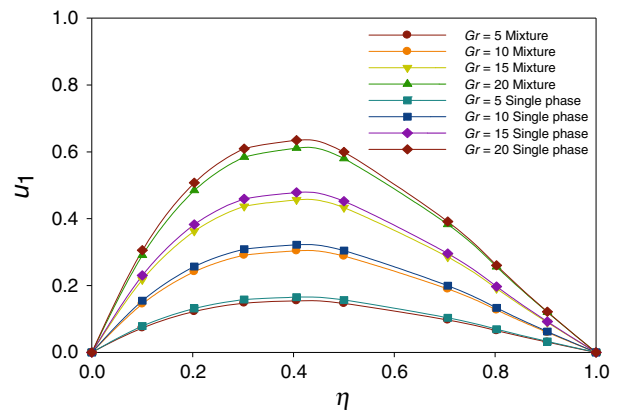
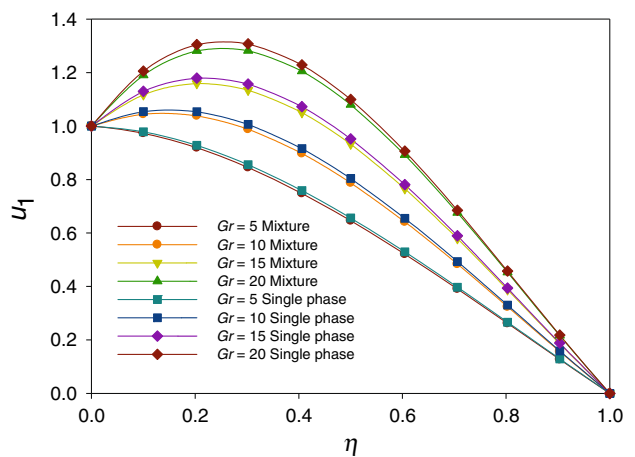


Fig. 10 Variations of dimensionless temperature in the channel width for moving plate and fixed plate and constant temperature (PST) boundary condition for $Gr = 5$, $Nr = 0.5$ and different volume fractions



(a) Fixed plate, PST boundary conditions



(b) Moving plate, PST boundary conditions

Fig. 11 Variations in dimensionless velocity in the channel width for condition of **a** fixed plate and constant temperature and **b** moving plate and constant temperature for $Nr = 0.5$, $\phi = 0.1\%$ and different Grashof numbers

Table 5 Comparison of dimensionless velocity for single-phase and two-phase models for constant temperature case and fixed and moving walls for volume fraction of $\phi = 0.1\%$, radiation number of $Nr = 0.5$ and different Grashof numbers

Boundary condition	Grashof number	Maximum deviation/%	Minimum deviation/%
Stationary wall and constant temperature	5	7.43	5.92
	10	6.81	3.95
	15	6.19	2.04
	20	5.58	0.19
Moving wall and constant temperature	5	1.62	0.008
	10	2.06	0.01
	15	2.09	0.019
	20	0.96	0.195

Effect of Grashof number on velocity

Figure 11 shows the variations of dimensionless velocity across the channel width for different Gr values in the constant temperature (PST) boundary condition for fixed and moving walls. In this diagram, the dimensionless temperature is shown for $Gr = 5, 10, 15$ and 20 , $Nr = 0.5$ and $\phi = 0.1$. For the fixed and moving plates by increasing Grashof number, the axial velocity of the fluid rises. Grashof number indicates the effect of buoyancy forces in natural convection. $Gr > 0$ indicates increasing density field gradients which result in higher buoyancy force. Increasing Grashof number results in inducing stronger secondary flows due to convection and higher acceleration of flow passing the channel. In Fig. 11, the velocity field in the single-phase simulation is estimated to be higher than the two-phase mixture method. The reason for this is lack of noticing and separation of velocity fields for solid and fluid phases and this parameter is suitably included in the two-phase method. Based on Fig. 11b, the presence of moving BC results in creation of secondary flows in the fluid field and the motion of the fluid will experience drift because density difference and the buoyancy caused by creation of secondary fluid are affected by velocity penetration caused by the moving plate in the fluid in that vicinity which will influence the entire fluid flow. By increasing Gr number, the dimensionless axial velocity rises and the maximum value for both fixed and moving plates moves toward the warm plate and the position of maximum velocity or velocity peak will be situated closer to the warm wall.

In Table 5, the single- and two-phase data are given for constant temperature case for fixed and moving walls for different Gr values for $\phi = 0.1$ and $Nr = 0.5$. The single-phase solution estimates higher velocities than the two-phase solution. By the investigation of the curve, it can be concluded that the maximum estimation error for the fixed plate is 7.43% and for moving plate it is 2.09% which

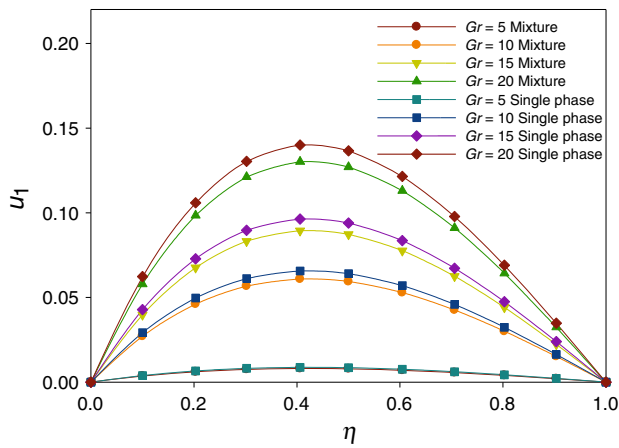
happen in $Gr = 5$ and 15 , respectively. In general, the axial velocity field shows lower sensitivity for moving plate BC for single- and two-phase solutions and in other words the application of two-phase model in the fixed plate results in higher errors and it appears that this BC will show better results for forced and mixed convection problems.

In Fig. 12, the numerical solution of flow field and heat transfer with two-phase mixture and single-phase methods for constant heat flux BC for fixed and moving plates is shown. This investigation is done for different Gr values and $Nr = 0.5$ and $\phi = 0.1\%$ solid nanoparticles. For the constant heat flux BC, because this BC is the same conditions and specifically in the same Gr value, the internal energy of the fluid is smaller in the heat flux case compared with constant temperature case; as a result, the secondary flows induced have a lower level in the constant heat flux BC compared with the constant temperature BC. As it is observed, similar to constant temperature diagrams the single-phase solution shows higher velocity values and by increasing Gr value, because of higher buoyancy force effects, higher velocities are achieved.

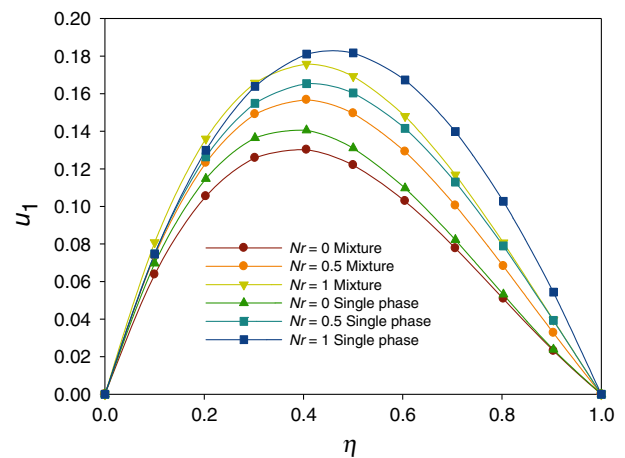
The minimum and maximum values are calculated for single- and two-phase cases for fixed and moving wall BCs for constant heat flux case in Table 6. The minimum velocity differences for fixed wall are close for single- and two-phase cases but the maximum values are strongly different, but there are no high variations in the moving plate case.

Effect of radiation parameter on velocity

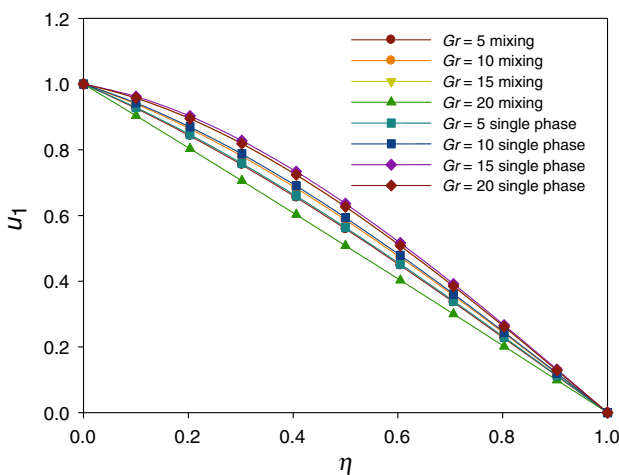
In Fig. 13, the variations of dimensionless velocity field for the two-phase mixture method and single-phase method are shown for determination of velocity profiles across channel width for different radiation parameters of 0, 0.5 and 1 for $Gr = 5$ and volume fraction of 0.1%, for constant temperature and moving constant plate. By increasing radiation number and because of reduced convective heat transfer



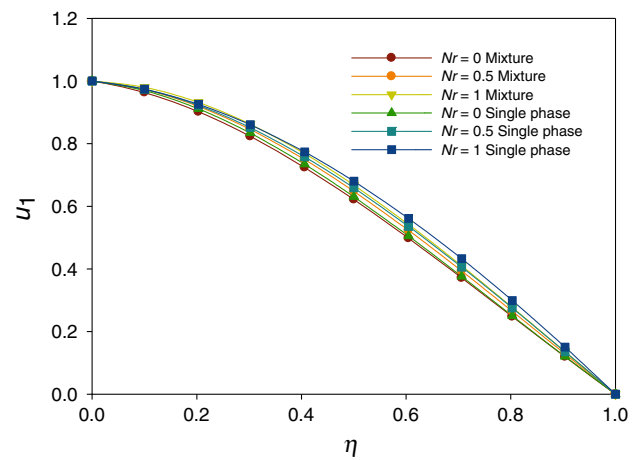
(a) Fixed plate, PHF boundary conditions



(a) Fixed plate, PST boundary conditions



(b) Moving plate, PHF boundary conditions



(b) Moving plate, PST boundary conditions

Fig. 12 Variations in dimensionless velocity in the channel width for condition of **a** fixed plate and constant heat flux and **b** moving plate and constant heat flux for $Nr = 0.5$, $\phi = 0.1\%$ and different Grashof numbers

Fig. 13 Variations in dimensionless velocity in the channel width for condition of **a** fixed plate and constant temperature and **b** moving plate and constant temperature for $Gr = 5$, $\phi = 0.1\%$ and different radiation numbers

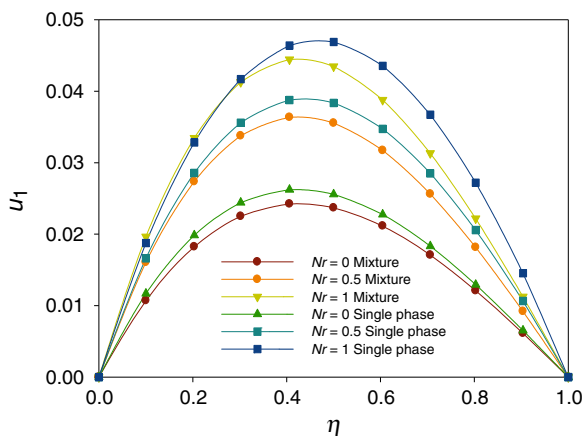
Table 6 Comparison of dimensionless velocity for single-phase and two-phase models for constant heat flux case and fixed and moving walls for volume fraction of $\phi = 0.1\%$, radiation number of $Nr = 0.5$ and different Grashof numbers

Boundary condition	Grashof number	Maximum deviation/%	Minimum deviation/%
Stationary wall and constant heat flux	5	8.01	7.81
	10	7.90	7.79
	15	7.84	7.47
	20	0.19	7.75
Stationary wall and constant heat flux	5	0.15	4e-4
	10	0.039	3e-3
	15	1.414	4e-3
	20	1.84	0.19

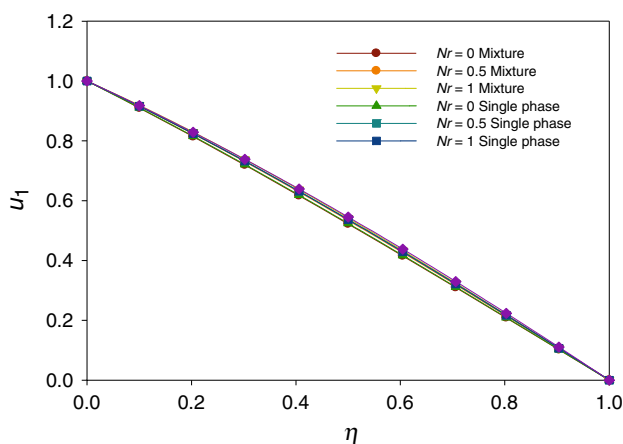
and higher radiation flux penetration in fluid layers, the fluid flow field temperature rises. With higher temperature in different fluid regions, density gradients grow stronger. This results in higher buoyancy force and inducement of secondary flows in the fluid flow field. Higher dimensionless velocity levels for fixed plate case are solely because of buoyancy force, but by increasing movement of warm plate, in addition to existence of buoyancy mechanism, the inducement of fluid velocity by plate motion results in a more significant growth in the dimensionless velocity profiles. By increasing radiation number, the maximum velocity increases. For the fixed plate by increasing radiation number, the maximum velocity moves toward the warmer wall and this is not observed for the moving plate. For the moving plate case, there is not much of a difference between flow field simulations in single- and two-phase methods but there is a difference in the fixed plate case.

This is because of lack of estimation of solid–fluid behavior in the single-phase method.

Figure 14 is similar to other considered cases and shows variations of axial velocity field. In this diagram, we first consider velocity field in two-phase and then in single-phase cases. For the constant heat flux BC and for fixed and moving plates, the problem is solved for $Nr = 0, 0.5$ and 1 for $\phi = 0.1\%$ and $Gr = 5$. For a given Nr value, the axial velocity curves are lower for constant heat flux BC compared with constant temperature. This is because of lower influence of temperature field in the constant flux case on the velocity parameter. For both curves by increasing Nr value, nanofluid becomes warmer and is accompanied by the formation of flow because of buoyancy force. In general, in the constant heat flux BC with moving plate the behavior of flow field is independent of single- or two-phase behavior of the flow and all curves are almost touching each other.



(a) Fixed plate, PHF boundary conditions



(b) Moving plate, PHF boundary conditions

Fig. 14 Variations in dimensionless velocity in the channel width for condition of **a** fixed plate and constant heat flux and **b** moving plate and constant heat flux for $Gr = 5$, $\phi = 0.1\%$ and different radiation numbers

Conclusions

In this study, a numerical simulation of effect of thermal radiation along with natural convection in steady state for a vertical channel with single-phase and two-phase mixture methods was carried out. These analyses were done for Grashof number of 5, 10, 15 and 20, radiation parameter of 0, 0.5 and 1 and volume fractions of 0, 0.1 and 0.2% copper solid nanoparticles with pure water as base fluid. The results showed that increasing volume fraction of solid nanoparticles has an inverse effect on variations of dimensionless temperature at the cross section for constant heat flux case (for moving and fixed plate cases) so that increasing volume fraction results in lower-temperature field and higher cooling. But for fixed plate case, the velocity of nanofluid at the walls is zero because of fixed position of the plate and presence of no-slip boundary condition on the solid walls. For both boundary conditions (constant heat flux and temperature), increasing solid nanoparticles volume fraction results in lowering the velocity contour elevations. The reason for this behavior is increased volume fraction of solid nanoparticles in the base fluid which results in higher viscous forces and density of coolant fluid and resulting a reduction in buoyancy force. The level of axial velocity curves in constant heat flux is about 2–3 times lower than constant temperature for $Gr = 5$ and $Nr = 0.5$. The reason for this behavior is that the constant temperature boundary condition applies more heat to the velocity field in the same Grashof number compared with constant heat flux case so that by increasing the applied temperature the value of kinetic and internal energy of the velocity field raises which results in higher density gradients and higher buoyancy forces. The

presence of moving plate boundary condition induces secondary flows in the flow field, and the flow movement in the channel will experience drift because of temperature variations and buoyancy forces due to inducement of secondary forces and the effect of penetration of moving plate velocity into the fluid close by it which will affect the entire fluid flow field in the end. For the constant heat flux case compared with constant temperature case, the velocity field is lower. The reason for this is the smaller effect of temperature field in the constant heat flux case on the velocity field.

References

1. Das S, Jana RN, Makinde OD. Transient natural convection in a vertical channel filled with nanofluids in the presence of thermal radiation. *Alex Eng J*. 2016;55:253–62.
2. Pantokratoras A. Natural convection along a vertical isothermal plate with linear and nonlinear Rosseland thermal radiation. *Int J Therm Sci*. 2014;84:151–7.
3. Hossain MA, Tashakor H. Radiation effect on mixed convection along a vertical plate with uniform surface temperature. *Heat Mass Transf*. 1996;31:243–9.
4. Das S, Mandal C, Jana RN. Effects of radiation on unsteady Couette flow between two vertical parallel plates. *Int J Comput Appl*. 2012;39:37–45.
5. Das K, Duari PR, Kundu PK. Numerical simulation of nanofluid flow with convective boundary condition. *J Egypt Math Soc*. 2015;23(2):435–9.
6. Dogonchi AS, Ganji DD. Thermal radiation effect on the nanofluid buoyancy flow and heat transfer over a stretching sheet considering Brownian motion. *J Mol Liq*. 2016;223:521–7.
7. Rashidi MM, Vishnu Ganesh N, Abdul Hakeem AK, Ganga B. Buoyancy effect on MHD flow of nanofluid over a stretching sheet in the presence of thermal radiation. *J Mol Liq*. 2014;198:234–8.
8. Pantokratoras A, Fang T. Sakiadis flow with nonlinear Rosseland thermal radiation. *Phy Scr J*. 2013;87:5–15.
9. Garoosi F, Rohani B, Rashidi MM. Two-phase mixture modeling of mixed convection of nanofluids in a square cavity with internal and external heating. *Powder Technol*. 2015;275:304–21.
10. Akbarinia A, Behzadmehr A. Numerical study of laminar mixed convection of a nanofluid in horizontal curved tubes. *Appl Therm Eng*. 2007;27:1327–37.
11. Mirmasoumi S, Behzadmehr A. Numerical study of laminar mixed convection of a nanofluid in a horizontal tube using two-phase mixture model. *Appl Therm Eng*. 2008;28:717–27.
12. Shariat M, Moghari RM, Akbarinia A, Rafee R, Sajjadi SM. Impact of nanoparticle mean diameter and the buoyancy force on laminar mixed convection nanofluid flow in an elliptic duct employing two phase mixture model. *Int Commun Heat Mass Transf*. 2014;50:15–24.
13. Oztop HF, Eiyad Abu-Nada MM, Hakan IP. heat line analysis of natural convection in a square inclined enclosure filled with a CuO nanofluid under non-uniform wall heating condition. *Int J Heat Mass Transf*. 2012;55:5076–86.
14. Xu H, Fan T, Pop I. Analysis of mixed convection flow of a nanofluid in a vertical channel with the Buongiorno mathematical model. *Int Commun Heat Mass Transf*. 2013;44:15–22.
15. Ahmed SE, Mansour MA, Hussein AK, Sivasankaran S. Mixed convection from a discrete heat source in enclosures with two adjacent moving walls and filled with micropolar nanofluids. *Eng Sci Technol Int J*. 2016;19(1):364–76.
16. Joshaghani M, Ghasemi-Fare O, Ghavami M. Experimental investigation on the effects of temperature on physical properties of sandy soils. *IFCEE 2018 GSP* 294.
17. Joshaghani M, Ghasemi-Fare O. A study on thermal consolidation of fine grained soils using modified consolidometer. *Geo-Congress 2019GSP* 309.
18. Khodabandeh E, Rozati SA, Joshaghani M, Akbari OA, Akbari S, Toghraie D. Thermal performance improvement in water nanofluid/GNP-SDBS in novel design of double-layer microchannel heat sink with sinusoidal cavities and rectangular ribs. *J Therm Anal Calorim*. 2018. <https://doi.org/10.1007/s10973-018-7826-2>.
19. Bakhshi H, Khodabandeh E, Akbari OA, Toghraie D, Joshaghani M, Rahbari A. Investigation of laminar fluid flow and heat transfer of nanofluid in trapezoidal microchannel with different aspect ratios. *Int J Numer Methods Heat Fluid Flow*. 2018. <https://doi.org/10.1108/HFF-05-2018-0231>.
20. Bahmani MH, Sheikhzadeh G, Zarringhalam M, Akbari OA, Alrashed AAAA, Shabani GAS, Goodarzi M. Investigation of turbulent heat transfer and nanofluid flow in a double pipe heat exchanger. *Adv Powder Technol*. 2018;29:273–82.
21. Rashidi MM, Nasiri M, Safdari Shadloo M, Yang Z. Entropy generation in a circular tube heat exchanger using nanofluids: effects of different modeling approaches. *Heat Transf Eng*. 2016. <https://doi.org/10.1080/01457632.2016.1211916>.
22. Maleki H, Safaei MR, Alrashed AAAA, Kasaeian A. Flow and heat transfer in non-Newtonian nanofluids over porous surfaces. *J Therm Anal Calorim*. 2018. <https://doi.org/10.1007/s10973-018-7277-9>.
23. Nasiri H, Abdollahzadeh Jamalabadi MY, Sadeghi R, Safaei MR, Nguyen TK, Safdari Shadloo M. A smoothed particle hydrodynamics approach for numerical simulation of nano-fluid flows. *J Therm Anal Calorim*. 2018. <https://doi.org/10.1007/s10973-018-7022-4>.
24. Moghaddaszadeh N, Esfahani JA, Mahian O. Performance enhancement of heat exchangers using eccentric tape inserts and nanofluids. *J Therm Anal Calorim*. 2019. <https://doi.org/10.1007/s10973-019-08009-x>.
25. Mahian O, Kolsi L, Amani M, Estellé P, Ahmadi G, Kleinstreuer C, Marshall JS, Siavashi M, Taylor RA, Niazmand H, Wongwises S, Hayat T, Kolanjijil A, Kasaeian A, Pop I. Recent advances in modeling and simulation of nanofluid flows—part I: fundamental and theory. *Phys Rep*. 2018. <https://doi.org/10.1016/j.physrep.2018.11.004>.
26. Mahian O, Kolsi L, Amani M, Estellé P, Ahmadi G, Kleinstreuer C, Marshall JS, Taylor RA, Abu-Nada E, Rashidi S, Niazmand H, Wongwises S, Hayat T, Kasaeian A, Pop I. Recent advances in modeling and simulation of nanofluid flows—part II. *Appl Phys Rep*. 2018. <https://doi.org/10.1016/j.physrep.2018.11.003>.
27. Safaei MR, Safdari Shadloo M, Goodarzi M, Hadjadj A, Goshayeshi HR, Afrand M, Kazi SN. A survey on experimental and numerical studies of convection heat transfer of nanofluids inside closed conduits. *Adv Mech Eng*. 2016;8(10):168781401667356.
28. Shadloo MS, Oger G, Le Touzé D. Smoothed particle hydrodynamics method for fluid flows, towards industrial applications: motivations, current state, and challenges. *Comput Fluid*. 2016;136:11–34.
29. Hopp-Hirschler M, Safdari Shadloo M, Nieken U. Viscous fingering phenomena in the early stage of polymer membrane formation. *J Fluid Mech*. 2019;864:97–140.
30. Sadeghi R, Shadloo MS, Hopp-Hirschler M, Hadjadj A, Nieken U. Three-dimensional lattice Boltzmann simulations of high density ratio two-phase flows in porous media. *Comput Math*

- Appl. 2018;75(7):2445–65. <https://doi.org/10.1016/j.camwa.2017.12.028>.
31. Sadeghi R, Shadloo MS. Three-dimensional numerical investigation of film boiling by the lattice Boltzmann method. *Numer Heat Transf Part A Appl.* 2017;71(5):560–74.
 32. Lebon B, Nguyen MQ, Peixinho J, Shadloo MS, Hadjadj A. A new mechanism for periodic bursting of the recirculation region in the flow through a sudden expansion in a circular pipe. *Phys Fluid.* 2018;30(3):031701.
 33. Nguyen MQ, Shadloo MS, Hadjadj A, Lebon B, Peixinho J. Perturbation threshold and hysteresis associated with the transition to turbulence in sudden expansion pipe flow. *Int J Heat Fluid Flow.* 2019;76:187–96.
 34. Esfe MH, Hassani Ahangar MR, Toghraie D, Hajmohammad MH, Rostamian H, Tourang H. Designing artificial neural network on thermal conductivity of Al₂O₃–water–EG (60–40%) nanofluid using experimental data. *J Therm Anal Calorim.* 2016;126(2):837–43.
 35. Alipour H, Karimipour A, Safaei MR, Semiromi DT, Akbari OA. Influence of T-semi attached rib on turbulent flow and heat transfer parameters of a silver-water nanofluid with different volume fractions in a three-dimensional trapezoidal microchannel. *Physica E.* 2016;88:60–76.
 36. Akbari OA, Toghraie D, Karimipour A. Numerical simulation of heat transfer and turbulent flow of water nanofluids copper oxide in rectangular microchannel with semi attached rib. *Adv Mech Eng.* 2016;8:1–25.
 37. Akbari OA, Hassanzadeh Afrouzi H, Marzban A, Toghraie D, Malekzade H, Arabpour A. Investigation of volume fraction of nanoparticles effect and aspect ratio of the twisted tape in the tube. *J Therm Anal Calorim.* 2017;129:1911–22.
 38. Manca O, Nardini S, Ricci D. A numerical study of nanofluid forced convection in ribbed channels. *Appl Therm Eng.* 2012;37:280–92.
 39. Oveissi S, Eftekhari SA, Toghraie D. Longitudinal vibration and instabilities of carbon nanotubes conveying fluid considering size effects of nanoflow and nanostructure. *Physica E.* 2016;83:164–73.
 40. Shamsi MR, Akbari OA, Marzban A, Toghraie D, Mashayekhi R. Increasing heat transfer of non-Newtonian nanofluid in rectangular microchannel with triangular ribs. *Physica E.* 2017;93:167–78.
 41. Akbari OA, Toghraie D, Karimipour A, Marzban A, Ahmadi GR. The effect of velocity and dimension of solid nanoparticles on heat transfer in non-Newtonian nanofluid. *Physica E.* 2017;86:68–75.
 42. Heydari M, Toghraie D, Akbari OA. The effect of semi-attached and offset mid-truncated ribs and Water/TiO₂ nanofluid on flow and heat transfer properties in a triangular microchannel. *Therm Sci Eng Prog.* 2017;2:140–50.
 43. Gravndyan Q, Akbari OA, Toghraie D, Marzban A, Mashayekhi R, Karimi R, Pourfattah F. The effect of aspect ratios of rib on the heat transfer and laminar water/TiO₂ nanofluid flow in a two-dimensional rectangular microchannel. *J Mol Liq.* 2017;236:254–65.
 44. Rahmati AR, Akbari OA, Marzban A, Toghraie D, Karimi R, Pourfattah F. Simultaneous investigations the effects of non-Newtonian nanofluid flow in different volume fractions of solid nanoparticles with slip and no-slip boundary conditions. *Therm Sci Eng Prog.* 2018;5:263–77.
 45. Parsaiemehr M, Pourfattah F, Akbari OA, Toghraie D, Sheikhzadeh Gh. Turbulent flow and heat transfer of water/Al₂O₃ nanofluid inside a rectangular ribbed channel. *Physica E.* 2018;96:73–84.
 46. Bejan A. *Convection heat transfer.* 3rd ed. Hoboken: Wiley; 2003.
 47. Mirmasoumi S, Behzadmehr A. Effect of nanoparticles mean diameter on mixed convection heat transfer of a nanofluid in a horizontal tube. *Int J Heat Fluid Flow.* 2008;29:557–66.
 48. Manninen M, Taivassalo V, Kallio S. On the mixture model for multiphase flow. Espoo: Technical Research Centre of Finland; 1996.
 49. Incropera FP, De Witt DP. *Introduction to heat transfer.* New York: Wiley; 2002.
 50. Akbari OA, Goodarzi M, Safaei MR, Zarringhalam M, Shabani GR, Dahari M. A modified two-phase mixture model of nanofluid flow and heat transfer in 3-d curved microtube. *Adv Powder Technol.* 2016;27:2175–85.
 51. Tavakoli MR, Akbari OA, Mohammadian A, Khodabandeh E, Pourfattah F. Numerical study of mixed convection heat transfer inside a vertical microchannel with two-phase approach. *J Therm Anal Calorim.* 2019;135(2):1119–34.
 52. Brinkman HC. The viscosity of concentrated suspensions and solutions. *J Chem Phys.* 1952;20:571.
 53. Khanafer K, Vafai K, Lightstone M. Buoyancy-driven heat transfer enhancement in a two-dimensional enclosure utilizing nanofluid. *Int J Heat Mass Transf.* 2003;46:3639–53.
 54. Rezaei O, Akbari OA, Marzban A, Toghraie D, Pourfattah F, Mashayekhi R. The numerical investigation of heat transfer and pressure drop of turbulent flow in a triangular microchannel. *Physica E.* 2017;93:179–89.
 55. Akbari OA, Karimipour A, Toghraie D, Safaei MR, Alipour H, Goodarzi M, Dahari M. Investigation of rib's height effect on heat transfer and flow parameters of laminar water–Al₂O₃ nanofluid in a two dimensional rib-microchannel. *Appl Math Comput.* 2016;290:135–53.
 56. Karimipour A, Alipour H, Akbari OA, Semiromi DT, Esfe MH. Studying the effect of indentation on flow parameters and slow heat transfer of water-silver nano-fluid with varying volume fraction in a rectangular two-dimensional micro channel. *Ind J Sci Technol.* 2016;8:45.
 57. Pourfattah F, Motamedian M, Sheikhzadeh Gh, Toghraie D, Akbari OA. The numerical investigation of angle of attack of inclined rectangular rib on the turbulent heat transfer of Water–Al₂O₃ nanofluid in a tube. *Int J Mech Sci.* 2017;131–132:1106–16.
 58. Barnoon P, Toghraie D. Numerical investigation of laminar flow and heat transfer of non-Newtonian nanofluid within a porous medium. *Powder Tech.* 2018;325:78–91.
 59. Toghraie D, Mahmoudi M, Akbari OA, Pourfattah F, Heydari M. The effect of using water/CuO nanofluid and L-shaped porous ribs on the performance evaluation criterion of microchannels. *J Therm Anal Calorim.* 2019;135(1):145–59.
 60. Mashayekhi R, Khodabandeh E, Bahiraei M, Bahrami L, Toghraie D, Akbari OA. Application of a novel conical strip insert to improve the efficacy of water–Ag nanofluid for utilization in thermal systems: a two-phase simulation. *Energy Convers Manag.* 2017;151:573–86.
 61. Maxwelle Garnett JC. Colours in metal glasses and in metallic films. *Philos Trans R Soc.* 1904;203:385–420.
 62. Haddad Z, Oztop HF, Abu-Nada E, Mataoui A. A review on natural convective heat transfer of nanofluids. *Renew Sustain Energy Rev.* 2012;16:5363–78.
 63. Arani AAA, Akbari OA, Safaei MR, Marzban A, Alrashed AAAA, Ahmadi GR, Nguyen TK. Heat transfer improvement of water/single-wall carbon nanotubes (SWCNT) nanofluid in a novel design of a truncated double layered microchannel heat sink. *Int J Heat Mass Transf.* 2017;113:780–95.
 64. Heydari A, Akbari OA, Safaei MR, Derakhshani M, Alrashed AA, Mashayekhi R, Shabani GA, Zarringhalam M, Nguyen TK. The effect of attack angle of triangular ribs on heat transfer of

- nanofluids in a microchannel. *J Therm Anal Calorim.* 2018;131(3):2893–912.
65. Gholami MR, Akbari OA, Marzban A, Toghraie D, Shabani GA, Zarringhalam M. The effect of rib shape on the behavior of laminar flow of oil/MWCNT nanofluid in a rectangular microchannel. *J Therm Anal Calorim.* 2018;134(3):1611–28.
66. Arabpour A, Karimipour A, Toghraie D, Akbari OA. Investigation into the effects of slip boundary condition on nanofluid flow in a double-layer microchannel. *J Therm Anal Calorim.* 2018;131(3):2975–91.
67. Toghraie D, Davood Abdollah MM, Pourfattah F, Akbari OA, Ruhani B. Numerical investigation of flow and heat transfer characteristics in smooth. Sinusoidal and zigzag-shaped microchannel with and without nanofluid. *J Therm Anal Calorim.* 2018;131:1757–66.
68. Sarlak R, Yousefzadeh S, Akbari OA, Toghraie D, Sarlak S, Assadi F. The investigation of simultaneous heat transfer of water/ Al_2O_3 nanofluid in a close enclosure by applying homogeneous magnetic field. *Int J Mech Sci.* 2017;133:674–88.

Publisher's Note Springer Nature remains neutral with regard to jurisdictional claims in published maps and institutional affiliations.